

Image Retrieval with Deep Local Features and Attention-based Keypoints

Hyeonwoo Noh*
POSTECH, Korea

André Araujo†
Google, Inc.

Jack Sim†
Google, Inc.

Bohyung Han*
POSTECH, Korea

Abstract

We introduce a local feature descriptor for large-scale image retrieval applications, called DELF (DEep Local Feature). The new feature is based on convolutional neural networks, which are trained without object- and patch-level annotations on a landmark image dataset. To enhance DELF’s image retrieval performance, we also propose an attention mechanism for keypoint selection, which shares most network layers with the descriptor. This new framework can be used in image retrieval as a drop-in replacement for other keypoint detectors and descriptors, enabling more accurate feature matching and geometric verification. Our technique is particularly useful for the large-scale setting, where a system must operate with high precision. In this case, our system produces reliable confidence scores to reject false positives effectively—in particular, our system is robust against queries that have no correct match in the database. We present an evaluation methodology for this challenging retrieval setting, using standard and large-scale datasets. We show that recently proposed methods do not perform well in this setup; DELF outperforms several recent global and local descriptors by substantial margins.

1. Introduction

Large-scale image retrieval is a fundamental task in computer vision, since it is directly related to various practical applications, *e.g.*, object detection, visual place recognition and product recognition. The last decades have witnessed tremendous advances in image retrieval systems—from hand-crafted features and indexing algorithms [20, 32, 25, 14] to, more recently, methods based on convolutional neural networks (CNN) for global descriptor learning [2, 27, 10].

Despite the recent advances in CNN-based global descriptors for image retrieval, they still suffer from the lack of ability to find patch-level matches between query and database images; it is difficult to handle partial occlusion and to distinguish similar instances of objects. In a different recent trend, CNN-based local features are proposed for patch-level

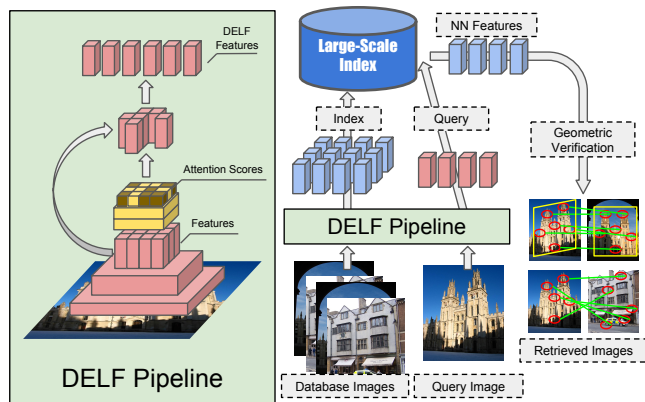


Figure 1: Overall architecture of our image retrieval system, using DEep Local Features (DELF) and attention-based keypoint selection. On the left, we illustrate the pipeline for extraction and selection of DELF features. The portion highlighted in yellow represents an attention mechanism which is trained to assign high scores to relevant features—features with the highest scores are selected. Feature extraction and selection can be performed with a single forward pass using our model. On the right, we illustrate our large-scale feature-based retrieval pipeline. DELF features for database images are indexed offline. The index supports querying by retrieving nearest neighbor (NN) features, which can be used to rank database images based on geometrically verified matches.

matching [11, 38, 36]. However, these techniques are not optimized specifically for image retrieval and show limited accuracy in practice. As a consequence, image retrieval systems relying on long-standing hand-crafted features, such as SIFT [20] or CONGAS [7], are still widely used.

The main goal of this work is to develop an image retrieval system with high precision and achieve outstanding performance for the large-scale image retrieval problem. We propose, as our first contribution, a CNN-based local feature which is designed specifically for large-scale image retrieval applications, as illustrated in Fig. 1. This new feature is called DELF (DEep Local Feature), and it is trained for instance-level recognition tasks without the need of object- and patch-level annotations. We show that DELF can be used with existing feature-based retrieval architectures as a drop-in replacement for hand-crafted descriptors, enabling image retrieval with geometrically verified feature matches.

Our second contribution is an attention mechanism for keypoint selection which improves the retrieval accuracy of

* {shgusdngogo, bhhan}@postech.ac.kr

† {andrearaujo, ssimzie}@google.com

systems which use DELF—the yellow part of the network in Fig. 1. The attention model is tightly coupled with the proposed descriptor; it reuses the same CNN architecture and generates feature scores using very little extra computation (in the spirit of recent advances in object detection [28]). This enables the extraction of both local descriptors and keypoints simply using one forward pass over the network.

Our third contribution is a thorough experimental evaluation for the retrieval scenario we are interested in, where high precision is required and robustness against queries that have no match in the database is very important. We test with standard and large-scale datasets, and show that recently proposed global and local descriptors do not perform well in this retrieval setting; DELF-based retrieval systems outperform them by significant margins.

2. Related Work

Instance retrieval has been a popular research problem for more than a decade. See [39] for a recent survey. Early systems relied on hand-crafted local features [20, 5, 7], coupled with approximate nearest-neighbor methods such as KD trees or vocabulary trees [6, 22, 24]. Still today, such feature-based techniques combined with geometric re-ranking provide strong performance when retrieval systems need to operate with high precision.

More recently, many works have focused on aggregation methods of local features, which include popular techniques such as VLAD [16] and Fisher Vector (FV) [17]. The main advantage of such global descriptors is the ability to provide high-performance image retrieval with a compact index.

In the past few years, several global descriptors based on CNNs have been proposed using pre-trained [4, 33] or learned networks [2, 27, 10]. These global descriptors are most commonly trained with a triplet loss, in order to preserve the ranking between relevant and irrelevant images. Some of these proposed CNN-based global descriptor methods make use of deep local features as a drop-in replacement for hand-crafted features in conventional aggregation techniques, such as VLAD or FV [37, 34]. Other works have re-evaluated and proposed different feature aggregation methods using such deep local features [3, 19].

CNNs have also been used to detect, represent and compare local image features. Verdie *et al.* [35] learned a regressor for repeatable keypoint detection. Yi *et al.* [21] proposed a generic CNN-based technique to estimate the canonical orientation of a local feature and successfully deployed it to several different descriptors. MatchNet [11] and Deep-Compare [38] have been proposed to jointly learn patch representations and associated metrics. Recently, LIFT [36] proposed an end-to-end framework to detect keypoints, estimate orientation and compute descriptors. Different from our work, these techniques are not designed for image retrieval applications and may suffer in this scenario.

Our algorithm employs deep neural networks to learn local feature descriptors for large-scale image retrieval. Contrary to previous works, we do not aggregate these features during indexing but construct a feature-based index, similar to [20]. This enables us to use deep local features with standard geometric verification methods, such as RANSAC [9]. In addition, while many recent methods have so far only been evaluated for moderate-sized datasets, in the order of hundreds of thousands of images, we focus on a large-scale evaluation of our approach, using a database with more than a million images and a query set with more than a hundred thousand images.

3. DELF Design

Our large-scale retrieval system can be decomposed into four main blocks: (i) dense localized feature extraction, (ii) keypoint selection, (iii) dimensionality reduction and (iv) indexing and retrieval. In this section, we describe in detail how DELF is extracted and trained. The feature-based indexing and retrieval stages are discussed in Sec. 5.

One unconventional aspect of our system is that keypoint selection comes after descriptor extraction. This is different from the traditional setting (*e.g.*, SIFT [20], CONGAS [7] or more recently LIFT [36]), where keypoints are first detected, and later described. While keypoints need to be repeatably detected under different imaging conditions, they also need to be sufficiently discriminative in order to distinguish among many different object instances. Not all repeatable keypoints are useful for discriminating object instances. Instead of designing a detector specifically for keypoint repeatability, we let the system learn to select features that directly improve instance recognition. One of the advantages of the proposed pipeline is that keypoint selection can be performed based on higher level semantics encoded in the dense feature maps, making it easier for discriminative features to be found. Our system does not require a separate keypoint detection stage, so feature selection can be performed at very little additional cost once descriptors are extracted.

3.1. Dense Localized Feature Extraction

Extraction. We extract dense features from an image by applying a fully convolutional network (FCN), which is constructed by using the feature extraction layers of a CNN trained with a classification loss. We employ an FCN taken from the ResNet50 [12] model, using the output of the *conv4_x* convolutional block. We use the parameters trained on ImageNet [29] as a baseline, and fine-tune them for an instance-level recognition task, as described in Sec. 3.2. To handle scale changes, we explicitly construct an image pyramid and apply the FCN for each level independently. The obtained feature maps are regarded as a dense grid of local descriptors.

Localization. Features are localized based on their receptive fields, which can be computed by considering the configuration of convolutional and pooling layers of the FCN. We use the image-level coordinates of the center of the receptive field as the feature location. The receptive field size for the image at the original scale is 291×291 . Using the image pyramid, we obtain features which describe image regions of different sizes.

3.2. Descriptor Fine-tuning

To enhance the discriminativeness of our local descriptors, we fine-tune them for an instance-level recognition task. In this work, we consider a landmark recognition application, so we use annotated datasets of landmark images. To set up the training process, we fine-tune the original ResNet50 model using these datasets, with a standard cross-entropy loss, as illustrated in Fig. 2 (a). The input images are initially center-cropped to produce square images, which are rescaled to 250×250 . Random 224×224 crops are then used in the training process.

As a result of this training process, local descriptors implicitly learn representations which are more relevant for the landmark retrieval problem. In this manner, no patch-level labels are necessary to obtain improved local descriptors.

3.3. Keypoint Selection

Instead of using densely extracted features directly for image retrieval, we design a technique to effectively select a subset of the features. Keypoint selection is important for both accuracy and computational efficiency of retrieval systems. A substantial part of the densely extracted features are irrelevant to our recognition task and add clutter, distracting the retrieval process. At the same time, the use of fewer features reduces memory consumption and system latency.

We estimate the importance of each feature using a score function, and select the features with highest scores. We also perform non-maximum suppression (NMS) in order to filter repeated features, where an intersection-over-union (IOU) threshold is employed to filter out features with low scores features that overlap significantly with high-scoring ones. We experiment with two types of score functions: (i) L_2 norm, and (ii) visual attention. In the following, we discuss the two methods.

3.3.1 Keypoint Selection by L_2 Norm

L_2 norm scoring measures the strength of activations for each feature, which can be seen as an indication of the presence of different object templates. If the network is trained for our instance-level recognition problem, the L_2 norm of the responses would provide a measure of the presence of discriminative features, making it a good candidate score function.

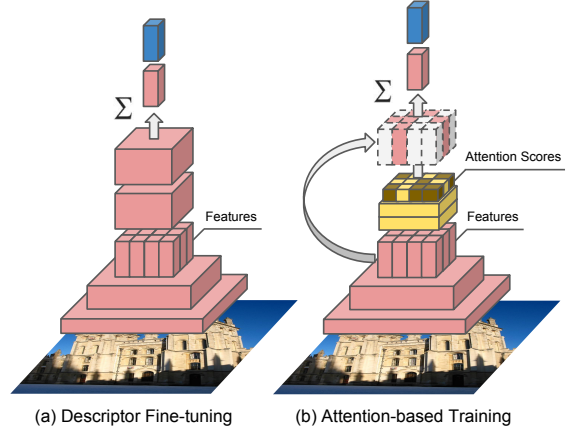


Figure 2: The network architecture used for (a) descriptor fine-tuning, on the left and (b) attention-based training, on the right.

3.3.2 Attention-based Keypoint Selection

We propose to train a function to explicitly learn relevance scores for local features. The training is set up in a similar manner as before (same loss function and datasets), and is illustrated in Fig. 2 (b)—where the attention network is highlighted in yellow. To train the landmark classifier, features are pooled by a weighted sum, where the weights are predicted by the attention network. This generates an embedding for the entire input image, which is then used to train a softmax-based landmark classifier.

More precisely, we formulate the training as follows. Denote by $\mathbf{f}_n \in \mathbb{R}^d, n = 1, \dots, N$ the d -dimensional features we are interested in learning together with the attention model. Our goal is to learn a score function $\alpha_{score}(\mathbf{f}_n)$ which produces a scalar for each feature. The output logit y of the network is generated by a weighted sum of feature vectors as follows:

$$\mathbf{y} = \mathbf{W} \left(\sum_n \alpha_{score}(\mathbf{f}_n) \cdot \mathbf{f}_n \right) \quad (1)$$

where $\mathbf{W} \in \mathbb{R}^{M \times d}$ represents the weights of the final fully-connected layer of the CNN trained to predict M classes.

We restrict the range of α_{score} to be non-negative, to prevent it from learning negative weighting. The score function is designed as a 2-layer CNN with a softplus [8] activation at the top. For simplicity, the convolutional filters are of size 1×1 , which works well in practice. At test time, each feature obtains an attention score, and we select the desired number of features with largest attention scores.

Note that, in this case, both the descriptors and the attention function are implicitly learned with image-level labels. This can pose some challenges to the learning process. While the feature representation and the score function can be trained jointly by back-propagation, we found that this setup does not work well in practice—it generates weak

models. Therefore, we employ a two-step training strategy: first, we learn descriptors with the fine-tuning process from Sec. 3.2; then, the score function is learned based on the fixed descriptors.

Another improvement to our models can be obtained by randomly scaling images during the training process. This is intuitive, as the attention model should be able to generate effective scores for features at different scales. We observed that this enables the learning of much more useful attention models in practice. In this case, the input images are initially center-cropped to produce square images, and rescaled to 900×900 . Random 720×720 crops are then extracted and finally randomly scaled with a factor $\gamma \leq 1$ to produce images with size 720×720 or smaller.

3.4. Dimensionality Reduction

We reduce the dimensionality of selected features to obtain improved retrieval accuracy, as common practice [13]. First, the selected features are L_2 normalized; then, PCA-based dimensionality reduction is applied; finally, the features once again undergo L_2 normalization.

4. Evaluation

The main application considered in our work is different from that of most existing image retrieval systems. We discuss two variants of objectives for image retrieval tasks, and describe how we verify the effectiveness of the proposed algorithm in the context of our focus.

4.1. Ranked vs. Unranked Image Retrieval

Image retrieval applications can be broadly categorized into two types: (i) ranked retrieval, and (ii) unranked retrieval. In the first case, systems return a list of results, ranked in descending order of relevance, so even loosely relevant items might be included in this list. An example of this type of application is web image search, where a user’s goal is often to explore potentially similar images to the query. The performance metric commonly used in this case, mean average precision (mAP), does not penalize returning more results, even if they are incorrect.

In the second type of application, unranked retrieval, a system is expected to return only the items that are relevant for a given query. The relevance score of each item in the database may not be reported. Usually, such systems must operate with high precision, in order to avoid exceeding a tolerable false positive rate. In this setup, it is very important to effectively handle distractor queries, *i.e.*, queries that have no relevant matches in the database, by simply not returning any result. In this setting, the absolute scores of database images for a given query are important, as only the images with sufficiently high scores should be returned. An example of this type of application is the automatic annotation of

personal photos with landmark labels, where the system should only suggest annotations with high confidence.

4.2. Performance Assessment

Our main focus is the unranked image retrieval problem. For proper evaluation of the target task, we measure the recall achieved at high precision operating points, for example, Recall@90% (in short, R@90%). To take distractor queries into account, precision and recall measures need to consider all queries together, since recall is not well-defined when evaluating retrieval results for a single distractor query. More precisely, for a given threshold τ to accept a retrieval match, denote the number of retrieved results for query q by R_q , the number of retrieved true positive results by R_q^{TP} , and the number of ground-truth true positive database images by G_q . We compute precision (P) and recall (R) respectively as:

$$P = \frac{\sum_{q=1}^Q R_q^{TP}}{\sum_{q=1}^Q R_q} \quad (2) \quad R = \frac{\sum_{q=1}^Q R_q^{TP}}{\sum_{q=1}^Q G_q} \quad (3)$$

where Q denotes the number of queries in the dataset.

5. Experiments

5.1. Experimental Setup

Retrieval datasets. The following standard datasets are used for most of the retrieval experiments.

- Oxford5k (Oxf5k) [25]: dataset of Oxford buildings containing 55 queries with bounding boxes, and 5,062 database images.
- Paris6k (Par6k) [26]: dataset of Paris buildings containing 55 queries with bounding boxes, and 6,412 database images.
- Flickr100k [25]: dataset containing 100k distractor images. As in previous work, we construct Oxford105k (Oxf105k) and Paris106k (Par106k) by adding Flickr100k images to the database of Oxf5k and Par6k, respectively.

In our evaluation using these datasets, we extract query features by first cropping the image and then processing the cropped image with each technique.

We evaluate two scenarios: (i) no distractor queries are used, as commonly done for these datasets; and (ii) distractor queries are used in each dataset. In the latter case, we use distractor queries as randomly selected images from a different dataset. For example, when using Oxf5k, we add Q^D Par6k images to the query set; in this case, the query set will contain a total of $Q^D + 55$ queries (55 from the original Oxf5k dataset, plus Q^D distractor queries selected among Par6k database images). We denote this dataset setting as Oxf5k*. Similarly, we construct Oxf105k* (similar to Oxf5k*, but with a larger database), Par6k* and Par106k* (where random database images from Oxf5k are used as distractor queries).

Scales	Parameters				Datasets	
	Keyp. Sel.	# Feat.	PCA	F.-tun.	Oxf5k*	Par6k*
1	-	-	-	-	6.27	4.08
0.25-1	-	-	-	-	18.78	13.98
0.25-1	L_2	1000	-	-	22.32	12.49
0.25-2	L_2	1000	-	-	33.91	30.35
0.25-2	L_2	1000	512	-	35.78	32.79
0.25-2	L_2	1000	128	-	38.71	34.82
0.25-2	L_2	1000	40	-	41.23	35.26
0.25-2	L_2	1000	40	SD	40.66	36.91
0.25-2	L_2	1000	40	LF	43.64	40.39
0.25-2	L_2	1000	40	LC	45.70	42.17
0.25-2	Att-LC	1000	40	LC	43.08	41.77
0.25-2	Att-LC+RS	1000	40	LC	42.63	39.68
0.25-2	Att-LF+RS	1000	40	LC	43.58	39.33
0.25-2	L_2 +Att-LC	1000	40	LC	46.07	40.86
0.25-2	L_2 +Att-LC+RS	1000	40	LC	45.14	40.56
0.25-2	L_2 +Att-LF+RS	1000	40	LC	46.72	41.09

Table 1: Retrieval results for variations of DELF, on the Oxf5k* and Par6k* datasets with $Q^D = 400$. We report R@90% in percentage.

Training datasets. The following datasets are used for fine-tuning descriptors and training keypoint selection.

- Landmarks dataset: introduced by Babenko *et al.* [4], we experiment with (i) the “full” version, referred to as LF (after removal of overlap classes with Oxf5k/Par6k, by Gordo *et al.* [10]), containing 140,372 images of 586 landmarks; and (ii) the “clean” version (LC), obtained with a SIFT-based matching procedure [10], with 35,382 images of 586 landmarks.
- siaMAC dataset (SD): originally introduced by Schonberger, *et al.* [30], this dataset was annotated in [27] using BoW and structure-from-motion techniques. It contains 22,156 images of 551 landmarks.

5.2. Evaluation of DELF Configurations

In this section, we present experiments to evaluate different configurations of our DELF descriptor, using Oxf5k* and Par6k*, with $Q^D = 400$. To perform image retrieval using DELF features, we follow a standard local descriptor based image retrieval methodology. First, we build a KD-tree index of all local descriptors extracted from database images. For efficiency reasons, we quantize each dimension of the descriptor uniformly into an 8-bit integer, as usually done in practice. For each local descriptor extracted from a query image, we perform approximate nearest neighbor search using best-bin-first [6] criterion until we visit T leaf nodes. Then for the top K nearest neighbor local descriptors retrieved from the index, we aggregate all the matches per dataset image. Finally, we perform geometric verification using RANSAC [9] and use the number of inliers as the score for retrieved images. We vary the retrieval parameters $K \in \{8, 16, 32, 64, 128\}$ and $T \in \{1280, 5000, 10000, 15000\}$ to obtain the best results for each configuration and report the best R@90% among the different parameter choices. Tab. 1 presents the overall results of these experiments, where we initialize the DELF

IOU threshold	0.5	0.7	1.0
Oxf5k*			
400 features	12.61	27.87	30.66
1000 features	15.91	27.88	33.91
Par6k*			
400 features	5.62	21.63	26.68
1000 features	6.60	20.15	30.35

Table 2: Retrieval performance (R@90% in percentage) for DELF- L_2 with “0.25-2” scales, as a function of the IOU threshold, for different number of selected features. In these experiments, $Q^D = 400$.

descriptor with a simple configuration and improve several building blocks one by one, to obtain high-accuracy features.

Multi-scale descriptor extraction. We construct image pyramids by using scales that are a $\sqrt{2}$ factor apart. For the set of scales with range from 0.25 to 1 (denoted as “0.25-1” in Tab. 1), 5 different scales are used; for “0.25-2”, 7 different scales are used. The receptive field’s side is reduced proportionally to the scale: for example, for the 0.25 scale, the receptive field is approximately of 73×73 pixels. Comparing “0.25-1” against single-scale processing, we observe a substantial performance improvement: R@90% triples.

L_2 keypoint selection. In our experiments, we noticed that non-discriminative features are discarded when using keypoint selection (*e.g.*, patches depicting sky or floor regions). This usually provides a boost in performance, especially when many scales are used. The use of “0.25-2” scales with L_2 keypoint selection enhances performance by more than 10% in both datasets, compared to the use of “0.25-1” scales. We also experimented with varying the number of selected features and observed that 1,000 is near-optimal for both datasets.

NMS. Tab. 2 presents results as the number of selected features and the IOU threshold are varied, using DELF- L_2 with “0.25-2” scales. Interestingly, for these two datasets, we do not observe retrieval improvements when suppressing non-max patches—the use of IOU threshold set to 1 is equivalent to not performing NMS. For all results reported in Tab. 1, we use 1,000 features without NMS.

PCA. As the dimensionality of our features is reduced using PCA, retrieval performance can be boosted substantially, similar to [13]. For Oxf5k* (Par6k*), the PCA-ed features improve retrieval by 7.32% (4.91%).

Descriptor fine-tuning. We compare retrieval results after performing fine-tuning on the training datasets. The SD dataset provides small if any improvements, while the LF and LC are much more effective. In particular, training on LC improves R@90% by more than 4% for both datasets.

Attention mechanism. We experimented with 3 different training settings: training on LC with and without the use of random scaling (RS), and training on LF with RS. Also, we experiment with using attention-based scores in two different ways: (i) by itself (denoted as Att); (ii) combined with L_2 norm score (denoted as L_2 +Att). In the latter case, both

scores are multiplied, and in many cases this generates a more robust keypoint selection score. For Oxf5k*, we observe a significant improvement when combining L_2 norm and attention scores, which suggests that they are complementary in this case. For Par6k*, attention-only score is better than combining attention with L_2 . L_2 +Att-LF+RS provides the best setting in Oxf5k*, with improvements of 1.02% over the use of L_2 norm selection. In Par6k*, performance actually degrades slightly (0.40%) when using attention, which is surprising. We have observed that attention-based selection is very helpful in large scale, as shown in Sec. 5.4.

Fig. 3 presents a visualization of the different keypoint selection methods, for some images. Qualitatively, it can be seen that the L_2 norm scores benefit from fine-tuning: scores for image regions without landmarks (e.g., faces, people) are suppressed, and scores for regions containing landmarks are boosted. A substantial difference can be observed between attention and L_2 scores: the attention portion of the network produces high scores for landmark regions while significantly suppressing clutter which is irrelevant for the landmark recognition task.

5.3. Comparison Against Other Techniques

DELf is compared against several recent global and local descriptors:

- Deep Image Retrieval (DIR) [10] is a recent global descriptor which obtains state-of-the-art performance for ranked image retrieval in several standard datasets. We use the released source code, which implements the version using ResNet101 [12], with 2,048 dimensions per global descriptor and multi-resolution descriptors in all cases. We also experiment with query expansion (QE), as reported in their work.
- siaMAC [27] is a recent global descriptor that obtains high performance in standard datasets. We use the released source code, which implements the version using VGG16 [31], with 512 dimensions per global descriptor. We also experiment with query expansion (QE), as reported in their work.
- CONGAS [7, 23] is a hand-engineered local feature which has been widely used for instance-level image matching and retrieval [40, 1]. CONGAS is extracted by collecting Gabor wavelet responses at the detected keypoint scale and orientation, and is known to have very similar performance and characteristic to other gradient-based local descriptors like SIFT. A Laplacian-of-Gaussian keypoint detector is used.
- LIFT [36] is a recently-proposed feature matching pipeline, where keypoint detection, orientation estimation and keypoint description are jointly learned. We use the source code released by the authors.

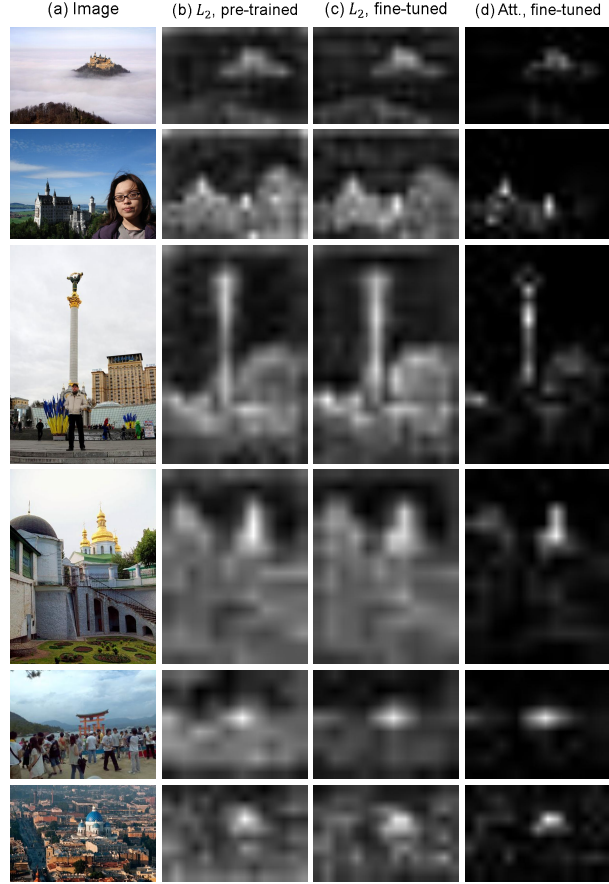


Figure 3: Visualization of the different keypoint selection methods. From left column: (a) input image; (b) L_2 norm scores using the pre-trained model; (c) L_2 norm scores using fine-tuned descriptors; (d) attention-based scores.

In this section, we use variants of DELf with “0.25-2” scales, fine-tuning on LC, and the attention mechanism learned on LF using random scaling. We use DELf with 40 dimensions (which is the same dimensionality of CONGAS). For comparable results against DIR, PCA is learned on the LC dataset. Note that LIFT is 128-dimensional. LIFT’s current implementation is slow, so we compare it against our techniques only on Oxf5k* and Par6k*. For DELf, CONGAS and LIFT, we use the exact same KD-tree based retrieval pipeline and parameter variations as described in Sec. 5.2, and a maximum of 1,000 features per image.

Tab. 3 presents results on standard datasets, with and without distractor queries. In this table, experiments with distractor queries use $Q^D = 800$. For the datasets without distractor queries, we report ranked retrieval performance measured by mAP. In this case, DIR outperforms other techniques, and its performance is boosted when using QE. DELf results fall in the same ballpark as DIR’s, although systematically lower—note that DIR uses ResNet101, while our model is based on ResNet50. Results for siaMAC are high, although lower than DIR—note that siaMAC uses VGG16 and only

Dataset	Oxf5k (mAP)	Oxf5k* (R@90%)	Oxf105k (mAP)	Oxf105k* (R@90%)
DIR [10]	86.07	51.43	82.75	5.24
DIR+QE [10]	87.08	10.93	85.30	0.44
siaMAC [27]	77.14	23.23	69.46	2.65
siaMAC+QE [27]	81.73	3.21	76.64	0.60
CONGAS [7]	70.80	42.39	61.10	12.47
LIFT [36]	53.96	21.98	-	-
DELFT- L_2 (ours)	84.44	43.86	83.47	10.90
DELFT-Att (ours)	83.79	40.49	82.62	12.02
DELFT- L_2 +Att (ours)	84.05	44.77	83.57	13.31
Dataset	Par6k (mAP)	Par6k* (R@90%)	Par106k (mAP)	Par106k* (R@90%)
DIR [10]	94.53	56.73	90.56	32.84
DIR+QE [10]	95.23	7.87	91.83	0.52
siaMAC [27]	83.94	27.19	76.27	0.52
siaMAC+QE [27]	86.24	0.91	79.77	0.38
CONGAS [7]	67.12	35.29	56.80	25.13
LIFT [36]	53.62	16.64	-	-
DELFT- L_2 (ours)	85.34	40.34	81.42	35.75
DELFT-Att (ours)	85.04	37.09	81.65	33.94
DELFT- L_2 +Att (ours)	84.77	38.24	81.27	35.44

Table 3: Retrieval performance on standard datasets, with and without distractor queries, for several different image retrieval techniques. In this table, experiments with distractor queries use $Q^D = 800$.

512 dimensions. Results for CONGAS and LIFT are clearly much worse for these datasets.

The main focus of this paper is the large-scale unranked retrieval case, where the datasets include distractor queries. Under these circumstances, the relative ranking between these algorithms changes substantially. Our proposed DELF variants outperform other techniques by a significant margin on Oxf105k* and Par106k*. These results indicate the importance of geometric verification for retrieval on such relatively large datasets: while global descriptors suffer substantially under these circumstances, DELF’s performance is much higher. It is interesting to note how the relative performance changes as the database grows, from Oxf5k* to Oxf105k*, or from Par6k* to Par106k*: DIR presents strong performance for the smaller datasets (even better than DELF in this case), but its performance quickly degrades as the database increases. In contrast, DELF’s performance degrades much more slowly.

Note that DELF also outperforms CONGAS in all cases; but, similarly to DELF, CONGAS’s performance also degrades much slower than DIR’s as the database grows. CONGAS’s results are similar to those reported in previous work using SIFT [20]: Philbin *et al.* [25] report 64.70% mAP on Oxf5k and 54.10% mAP on Oxf105k, when using a BoW-based approach with large vocabularies and geometric verification. Although our retrieval system is different from the one proposed by [25] (we use a KD-tree, while [25] uses BoW with large vocabularies), the fact that their results are similar to the ones reported for CONGAS in this paper suggests that both techniques perform similarly.

Another interesting observation is the strong degradation in performance of DIR+QE (and siaMAC+QE) when distractor queries are considered. This happens because QE

Oxf105k*	Q^D	0	400	800	1600
	r	0	7.27	14.54	29.09
Oxf105k*	Q^D	0	400	800	1600
DIR [10]		63.02	10.40	5.24	2.91
DELFT- L_2 (ours)		55.57	22.79	10.90	6.92
DELFT-Att (ours)		51.41	24.57	12.02	6.73
DELFT- L_2 +Att (ours)		55.67	24.12	13.31	6.09
Par106k*	Q^D	0	400	800	1600
	r	0	7.27	14.54	29.09
Par106k*	Q^D	0	400	800	1600
DIR [10]		51.61	40.48	32.84	19.62
DELFT- L_2 (ours)		45.17	38.32	35.75	30.89
DELFT-Att (ours)		43.84	35.91	33.94	28.04
DELFT- L_2 +Att (ours)		44.78	36.57	35.44	28.06

Table 4: Retrieval performance on standard datasets (R@90%), with a varying number of distractor queries (Q^D) on Oxf105k* (top) and Par106k* (bottom). r denotes the ratio between the number of distractor queries and the number of non-distractor queries for each configuration.

tends to retrieve database images that are similar to the ones retrieved in the first round of querying. For the case of distractor queries, where no database image is relevant, this leads the system to retrieve irrelevant images with high confidence scores. DELF and CONGAS are much more robust to distractor queries, showing the advantages of re-ranking with feature-based geometric verification, instead of QE.

We also present experimental results as number of distractor queries Q^D varies. Results are presented in Tab. 4, where r denotes the ratio between the number of distractor queries and the number of non-distractor queries for each configuration. It is clear that the DELF variants outperform DIR when there are many distractor queries, for both Oxf105k* and Par106k*. In Oxf105k*, DELF outperforms DIR significantly for $Q^D \geq 400$ (performance more than doubles in these cases). For Par106k*, DELF outperforms DIR for $Q^D \geq 800$; for $Q^D = 1600$, DELFT- L_2 outperforms DIR by 57% relative improvement. This demonstrates that DELF is more robust to datasets where distractor queries are abundant, as it is the case in practice for many unranked image retrieval applications.

5.4. Large-scale Experiments

In this section, we present a comparison of DELF against other methods in large scale. The application illustrated here is the annotation of photos from personal collections with recognized landmarks. In this case, it is very important that labels be assigned only if the system is very confident of a match.

Dataset. We use a private image database constructed using the algorithm described in [40]. It contains 1,060,709 images of 12,894 landmarks. For querying this dataset, we use 111,036 images from personal photo collections.

Performance assessment. Query and database images contain GPS annotations. However, we observed that this information is noisy, due to GPS errors and the fact that many images are manually annotated. Also, photos can be captured from a large distance for some landmarks (*e.g.*, Eiffel

Tower, Golden Gate Bridge)—so, in some cases the photo location might be relatively far from the actual landmark location. As a consequence, we consider a match to be correct if the retrieved landmark’s location is within 25km of the query image. In preliminary experiments, we observed that this generates very few incorrect annotations, so is appropriate for evaluation. Since there are very few true matches (as most query images do not depict any landmark), we report results by measuring the number of retrieved true positives at specific precision rates. More specifically, reusing the notation from Sec. 5.1, we define: $TP = \sum_{q=1}^Q R_q^{TP}$. We report TP for high precision rates—*e.g.*, for a precision rate of 90%, we report TP@90%. This measure is within a factor of the true recall (as computed by (3)), and it is simpler to report since the exact number of ground-truth images in the database does not need to be known.

Implementation. For this experiment, we implement a more scalable approach than KD-tree for retrieval using DELF and CONGAS: we encode each of our 40D descriptors to a 50-bit code using Product Quantization [15]. We split 40D descriptors into 10 chunks which are 4D each, then use $32 = 2^5$ k-means centroids per each sub-dimension to achieve 50-bit encoding. We perform asymmetric distance calculation, where we do not encode the query descriptors to improve the accuracy of nearest neighbor retrieval. To speed up the nearest neighbor search, we construct an inverted index for descriptors, using a codebook of size 8,000. To avoid a large encoding error, instead of applying a single quantization model per inverted list entry, each inverted list is composed into a KD-tree which utilizes Locally Optimized Product Quantizers [18]. This pipeline requires less than 8GB of RAM to index 1 billion descriptors, which is sufficient to index our large-scale landmark dataset. The latency of the nearest neighbor search is less than 2 seconds using a single CPU under our experiment setup, where we soft-assign 5 centroids for each query and search up to 10,000 leaf nodes within each inverted index tree. To make the DELF variants even more amenable to large scale, we reduce the number of features per image to 500 and filter out any feature with a keypoint selection score less than 0.01. The effect of these two parameters is analyzed in detail in the appendices.

For DIR, we use a parallelized implementation of brute-force search—to avoid penalizing it with inaccuracies of approximate nearest neighbor search. As presented in Sec. 5.3, QE degrades global descriptor performance in the retrieval setting we consider, so we do not present results for DIR with QE in this section (we performed this experiment and confirmed that QE degrades performance substantially in this large-scale setting).

Results. Fig. 4 presents the precision-TP curve for this experiment, and Tab. 5 shows TP at high precision values. It is clear that the DELF variants which use attention-based

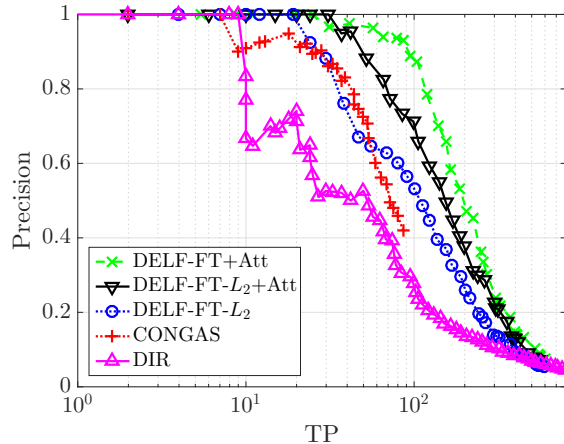


Figure 4: Precision-TP curve for the large-scale retrieval experiment.

Method	TP@95%	TP@90%	TP@85%
DIR [10]	9.29	9.59	9.89
CONGAS [7]	17.44	28.44	35.59
DELF-FT- L_2 (ours)	22.23	27.38	32.09
DELF-FT+Att (ours)	61.87	92.61	108.5
DELF-FT- L_2 +Att (ours)	42.59	49.42	59.75

Table 5: Comparison of our DELF descriptor variants against CONGAS and DIR, on our large-scale landmark dataset.

keypoint selection outperform substantially all other techniques. Considering TP@90%, DELF-FT+Att outperforms (in terms of relative improvement) DIR by 865.69%, CONGAS by 225.63%, DELF-FT- L_2 by 238.24% and DELF-FT- L_2 +Att by 87.39%. DIR suffers significantly at high precision, which indicates that many false matches obtain high score. CONGAS and DELF-FT- L_2 perform very similarly at high precision ranges, and DELF-FT- L_2 outperforms CONGAS for higher TP rates. Qualitative results are presented in the appendices, highlighting the strengths and weaknesses of these techniques.

6. Conclusion

In this work, we are interested in large-scale high-precision image retrieval applications. We propose DELF, a new local feature which is designed specifically for this problem. DELF is learned for an instance-level recognition task, and can be coupled to a new attention mechanism for effective and efficient feature selection. In our CNN-based model, one forward pass over the network is sufficient to obtain both keypoints and descriptors. We present several experiments, using standard and large-scale datasets. While global descriptors present high performance when using a common retrieval evaluation setup, we show that they suffer substantially when distractor queries are present. DELF obtains much better performance in this scenario, since it can use robust local feature matching scores. DELF also outperforms an effective hand-crafted local descriptor by a substantial margin in this setting.

Appendix A: Additional Experiments

In this section, we present further experimental results on our large-scale dataset, with different configurations for the indexing and retrieval stages.

Varying number of features. Tab. 6 presents results for DELF-FT- L_2 when using a different number of features for indexing and querying. For this large-scale dataset, it is more effective to avoid too many features per image – the best performance in this case is achieved with 400 features per image. This reflects the fact that the query set contains many distractors, and as a consequence the use of a large number of indiscriminative features might generate too many false feature matches.

Absolute threshold for feature selection. We also experiment with a feature selection threshold, to avoid using features that are weak and more likely to generate false matches. This enables the use of fewer features for images which do not contain many discriminative regions. In this case, features are discarded if their score is lower than a threshold β (the case where $\beta = 0$ corresponds to not discarding any feature based on their scores). For this experiment, we set the maximum number of features as 500.

Tab. 7 presents retrieval results, showing that it is important to discard features with small scores: performance is improved in all cases with $\beta = 0.01$, compared to $\beta = 0$. The improvement is most dramatic for DELF-FT+Att, in which case TP@90% more than doubles.

Appendix B: Qualitative Results

In this section, we present qualitative results to visually assess the main techniques compared in the paper. In the different figures, we present top-1 results retrieved by the different methods.

DELF vs DIR. Fig. 5 presents retrieval results where DELF outperforms DIR. DELF is able to obtain matches between specific local regions in images, which helps significantly for finding the same object in different imaging conditions. Common failure cases of DIR happen when the database contains generally similar objects or scenes, which is common in large scale – *e.g.*, obelisks, mountains, harbors, as illustrated in Fig. 5. In many cases, DIR cannot distinguish these specific objects or scenes; although it is able to find semantically similar images, often they do not correspond to the instance of interest. Another weakness of DIR (and any global descriptor) is naturally the lack of localization, which leads it to miss matches when the object of interest is small.

Fig. 6 shows cases where DIR outperforms DELF. DELF is able to match very localized patterns across different images, but this can lead to errors when the floor tiling or vegetation is similar across different locations.

DELF vs CONGAS. Fig. 7 presents query-database pairs

Method	# Feat.	TP@95%	TP@90%	TP@85%
DELF-FT- L_2	400	24.89	29.44	33.99
DELF-FT- L_2	500	19.67	21.36	23.02
DELF-FT- L_2	600	17.26	19.54	21.81
DELF-FT- L_2	1000	15.13	17.27	19.42

Table 6: Retrieval results on our large-scale dataset, evaluating the use of different numbers of features, without non-max suppression.

Method	β	TP@95%	TP@90%	TP@85%
DELF-FT- L_2	0	19.67	21.36	23.02
	0.01	22.23	27.38	32.09
	0.1	15.41	16.84	18.22
DELF-FT+Att	0	22.14	35.98	41.47
	0.01	61.87	92.61	108.5
	0.1	43.45	48.52	101.61
DELF-FT- L_2 +Att	0	34.41	35.84	46.29
	0.01	42.59	49.42	59.75
	0.1	26.37	44.79	58.54

Table 7: Retrieval results on our large-scale dataset, evaluating the use of an absolute threshold for feature selection, using a maximum of 500 features per image, without non-max suppression.

which are successful DELF matches, missed by CONGAS. DELF’s main improvement over CONGAS is in terms of recall: it is able to retrieve many more relevant landmarks compared to CONGAS. This suggests that DELF descriptors are more discriminative. We did not observe significant examples where CONGAS outperforms DELF, so we do not include such examples here.

In Fig. 7, we present feature correspondences by connecting the center of the receptive fields for matching features. Note that the receptive fields can be quite large. This explains why some features seem to be localized in indiscriminative regions (*e.g.*, in the ocean or in the sky) – in these cases, the features are extracted from large patches, which take into account more discriminative regions in its neighborhood.

Appendix C: Implementation Details

We provide more details on the experimental setup for the different techniques which are compared in the paper.

Deep Image Retrieval (DIR). The source code is available online ¹. For query expansion experiments, the query descriptor used in the second round is the average between the descriptor from the initial query and the descriptor from the top retrieved image in the first round. With this configuration, we are able to achieve very similar results to the ones reported by the authors [10].

LIFT. The source code is available online ². We used the default configuration of parameters in our experiments.

¹<http://www.xrce.xerox.com/Research-Development/Computer-Vision/Learning-Visual-Representations/Deep-Image-Retrieval>

²<https://github.com/cvlab-epfl/lift>



Figure 5: Visualization of examples where DELF-FT- L_2 +Att outperforms DIR. From the left column: (a) query image; (b) top-1 retrieved image of DELF-FT- L_2 +Att; (c) top-1 retrieved image of DIR. The green border denotes that the result is correct and the red border denotes that the result is incorrect.

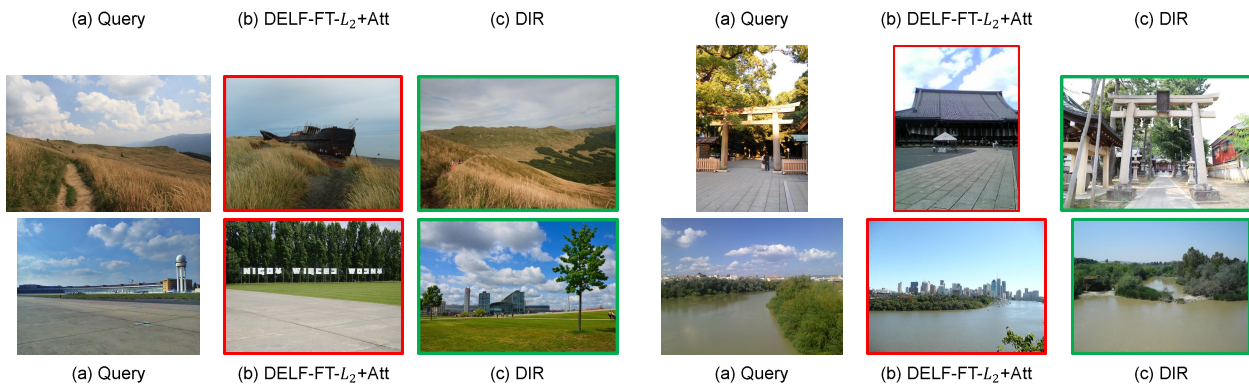


Figure 6: Visualization of examples where DIR outperforms DELF-FT- L_2 +Att. From the left column: (a) query image; (b) top-1 retrieved image of DELF-FT- L_2 +Att; (c) top-1 retrieved image of DIR. The green border denotes that the result is correct and the red border denotes that the result is incorrect.

CONGAS. We use an in-house implementation of CONGAS, which has been optimized for large-scale retrieval.

siaMAC. The source code is available online³. We use the exact same configuration for query expansion as the one used for DIR: the query descriptor used in the second round is the average between the descriptor from the initial query and the descriptor from the top retrieved image in the first round. With this configuration, we are able to achieve

³<http://cmp.felk.cvut.cz/~radenfil/projects/siamac.html>

very similar results to the ones reported by the authors [27], without the need to perform the additional re-ranking step from [33].

References

- [1] H. Aradhye, G. Toderici, and J. Yagnik. Video2text: Learning to Annotate Video Content. In *Proc. IEEE International Conference on Data Mining Workshops*, 2009. 6
- [2] R. Arandjelović, P. Gronat, A. Torii, T. Pajdla, and J. Sivic. NetVLAD: CNN Architecture for Weakly Supervised Place

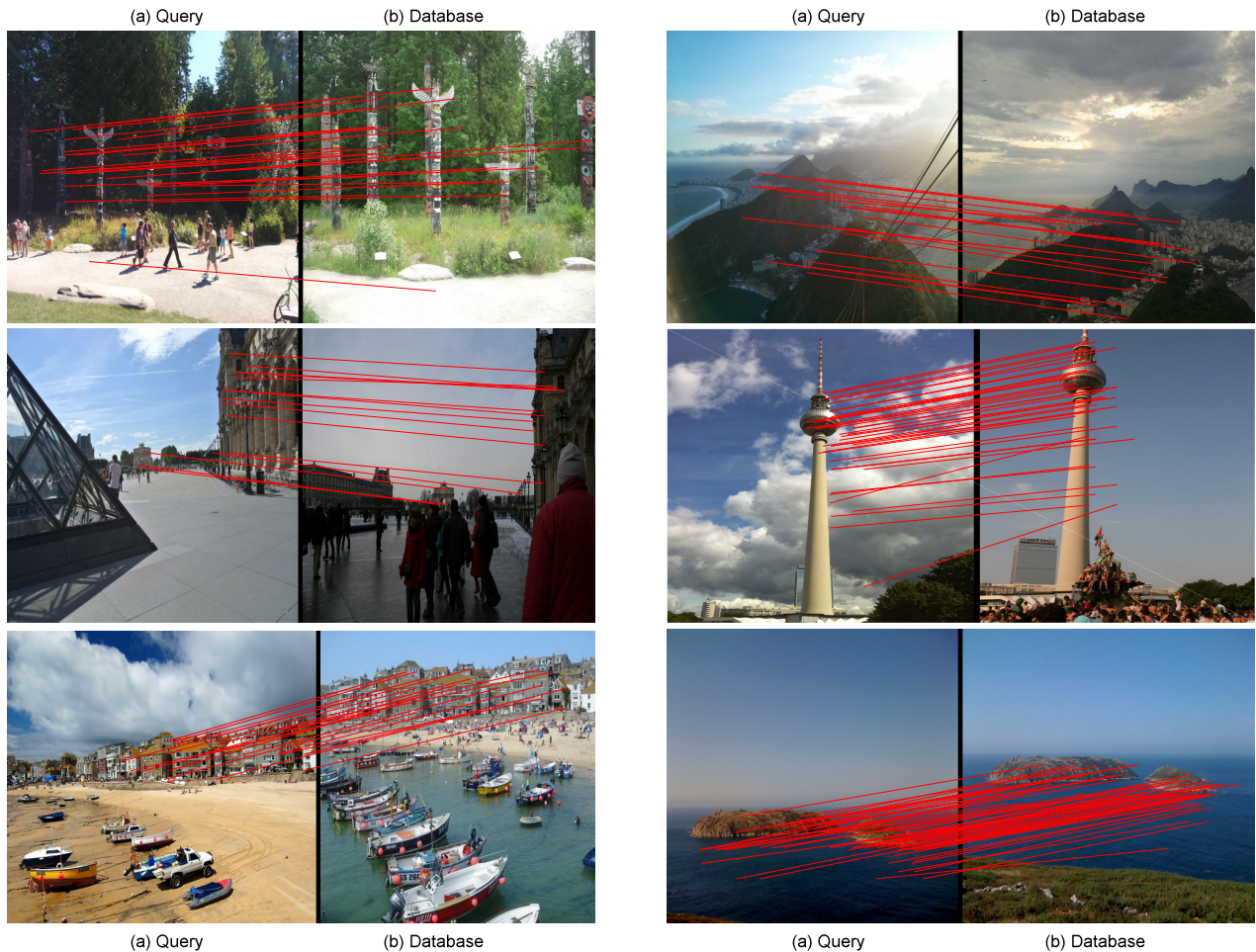


Figure 7: Visualization of feature correspondences found for query-database image pairs, using DELF-FT- L_2 +Att. For these queries, CONGAS did not retrieve any database image. From the left column: (a) query image; (b) database image.

- Recognition. In *Proc. CVPR*, 2016. 1, 2
- [3] A. Babenko and V. Lempitsky. Aggregating Local Deep Features for Image Retrieval. In *Proc. ICCV*, 2015. 2
- [4] A. Babenko, A. Slesarev, A. Chigorin, and V. Lempitsky. Neural Codes for Image Retrieval. In *Proc. ECCV*, 2014. 2, 5
- [5] H. Bay, A. Ess, T. Tuytelaars, and L. Van Gool. Speeded-Up Robust Features (SURF). *Computer Vision and Image Understanding*, 110(3):346–359, 2008. 2
- [6] J. S. Beis and D. G. Lowe. Shape Indexing Using Approximate Nearest-Neighbour Search in High-Dimensional Spaces. In *Proc. CVPR*, 1997. 2, 5
- [7] U. Buddemeier and H. Neven. Systems and Methods for Descriptor Vector Computation, 2012. US Patent 8,098,938. 1, 2, 6, 7, 8
- [8] C. Dugas, Y. Bengio, C. Nadeau, and R. Garcia. Incorporating Second-Order Functional Knowledge for Better Option Pricing. In *Proc. NIPS*, 2001. 3
- [9] M. Fischler and R. Bolles. Random Sample Consensus: A Paradigm for Model Fitting with Applications to Image Analysis and Automated Cartography. *Communications of the ACM*, 24(6):381–395, 1981. 2, 5
- [10] A. Gordo, J. Almazan, J. Revaud, and D. Larlus. Deep Image Retrieval: Learning Global Representations for Image Search. In *Proc. ECCV*, 2016. 1, 2, 5, 6, 7, 8, 9
- [11] X. Han, T. Leung, Y. Jia, R. Sukthankar, and A. C. Berg. MatchNet: Unifying Feature and Metric Learning for Patch-Based Matching. In *Proc. CVPR*, 2015. 1, 2
- [12] K. He, X. Zhang, S. Ren, and J. Sun. Deep Residual Learning for Image Recognition. In *Proc. CVPR*, 2016. 2, 6
- [13] H. Jégou and O. Chum. Negative Evidences and Co-Occurrences in Image Retrieval: The Benefit of PCA and Whitening. In *Proc. ECCV*, 2012. 4, 5
- [14] H. Jégou, M. Douze, and C. Schmid. Hamming Embedding and Weak Geometric Consistency for Large Scale Image Search. In *Proc. ECCV*. Springer, 2008. 1
- [15] H. Jégou, M. Douze, and C. Schmid. Product Quantization for Nearest Neighbor Search. *IEEE Transactions on Pattern Analysis and Machine Intelligence*, 33(1), 2011. 8

- [16] H. Jégou, M. Douze, C. Schmidt, and P. Perez. Aggregating Local Descriptors into a Compact Image Representation. In *Proc. CVPR*, 2010. 2
- [17] H. Jégou, F. Perronnin, M. Douze, J. Sanchez, P. Perez, and C. Schmid. Aggregating Local Image Descriptors into Compact Codes. *IEEE Transactions on Pattern Analysis and Machine Intelligence*, 34(9), 2012. 2
- [18] Y. Kalantidis and Y. Avrithis. Locally Optimized Product Quantization for Approximate Nearest Neighbor Search. In *Proc. CVPR*, 2014. 8
- [19] Y. Kalantidis, C. Mellina, and S. Osindero. Cross-Dimensional Weighting for Aggregated Deep Convolutional Features. In *Proc. ECCV Workshops*, 2015. 2
- [20] D. Lowe. Distinctive Image Features from Scale-Invariant Keypoints. *International Journal of Computer Vision*, 60(2), 2004. 1, 2, 7
- [21] K. Moo Yi, Y. Verdie, P. Fua, and V. Lepetit. Learning to Assign Orientations to Feature Points. In *Proc. CVPR*, 2016. 2
- [22] M. Muja and D. G. Lowe. Fast Approximate Nearest Neighbors with Automatic Algorithm Configuration. In *Proc. VISAPP*, 2009. 2
- [23] H. Neven, G. Rose, and W. G. Macready. Image Recognition with an Adiabatic Quantum Computer I. Mapping to Quadratic Unconstrained Binary Optimization. *arXiv:0804.4457*, 2008. 6
- [24] D. Nistér and H. Stewenius. Scalable Recognition with a Vocabulary Tree. In *Proc. CVPR*, 2006. 2
- [25] J. Philbin, O. Chum, M. Isard, J. Sivic, and A. Zisserman. Object Retrieval with Large Vocabularies and Fast Spatial Matching. In *Proc. CVPR*, 2007. 1, 4, 7
- [26] J. Philbin, O. Chum, M. Isard, J. Sivic, and A. Zisserman. Lost in Quantization: Improving Particular Object Retrieval in Large Scale Image Databases. In *Proc. CVPR*, 2008. 4
- [27] F. Radenović, G. Tolias, and O. Chum. CNN Image Retrieval Learns from BoW: Unsupervised Fine-Tuning with Hard Examples. In *Proc. ECCV*, 2016. 1, 2, 5, 6, 7, 10
- [28] S. Ren, K. He, R. Girshick, and J. Sun. Faster R-CNN: Towards Real-Time Object Detection with Region Proposal Networks. In *Proc. NIPS*, 2015. 2
- [29] O. Russakovsky, J. Deng, H. Su, J. Krause, S. Satheesh, S. Ma, Z. Huang, A. Karpathy, A. Khosla, M. Bernstein, et al. ImageNet Large Scale Visual Recognition Challenge. *International Journal of Computer Vision*, 115(3), 2015. 2
- [30] J. L. Schönberger, F. Radenović, O. Chum, and J.-M. Frahm. From Single Image Query to Detailed 3d Reconstruction. In *Proc. CVPR*, 2015. 5
- [31] K. Simonyan and A. Zisserman. Very Deep Convolutional Networks for Large-Scale Image Recognition. In *Proc. ICLR*, 2015. 6
- [32] J. Sivic and A. Zisserman. Video Google: A Text Retrieval Approach to Object Matching in Videos. In *Proc. ICCV*, 2003. 1
- [33] G. Tolias, R. Sircé, and H. Jégou. Particular Object Retrieval with Integral Max-Pooling of CNN Activations. In *Proc. ICLR*, 2015. 2, 10
- [34] T. Uricchio, M. Bertini, L. Seidenari, and A. Bimbo. Fisher Encoded Convolutional Bag-of-Windows for Efficient Image Retrieval and Social Image Tagging. In *Proc. ICCV Workshops*, 2015. 2
- [35] Y. Verdie, K. M. Yi, P. Fua, and V. Lepetit. TILDE: A Temporally Invariant Learned Detector. In *Proc. CVPR*, 2015. 2
- [36] K. M. Yi, E. Trulls, V. Lepetit, and P. Fua. LIFT: Learned Invariant Feature Transform. In *Proc. ECCV*, 2016. 1, 2, 6, 7
- [37] J. Yue-Hei Ng, F. Yang, and L. S. Davis. Exploiting Local Features from Deep Networks for Image Retrieval. In *Proc. CVPR Workshops*, 2015. 2
- [38] S. Zagoruyko and N. Komodakis. Learning to Compare Image Patches via Convolutional Neural Networks. In *Proc. CVPR*, 2015. 1, 2
- [39] L. Zheng, Y. Yang, and Q. Tian. SIFT Meets CNN: A Decade Survey of Instance Retrieval. *arXiv:1608.01807*, 2016. 2
- [40] Y.-T. Zheng, M. Zhao, Y. Song, H. Adam, U. Buddemeier, A. Bissacco, F. Brucher, T.-S. Chua, and H. Neven. Tour the World: Building a Web-Scale Landmark Recognition Engine. In *Proc. CVPR*, 2009. 6, 7